HHS Public Access

Author manuscript

Biomaterials. Author manuscript; available in PMC 2021 July 01.

Published in final edited form as:

Biomaterials. 2020 July ; 248: 120032. doi:10.1016/j.biomaterials.2020.120032.

Redirecting extracellular proteases to molecularly guide radiosensitizing drugs to tumors

Dina V. Hingorani[1,#], **Jessica L. Crisp**[2,#], **Matthew K. Doan**[1], **Maria F. Camargo**[1], **Maryam A. Quraishi**[1], **Joseph Aguilera**[1], **Mara Gilardi**[2], **Larry A. Gross**[2], **Tao Jiang**[2], **Wei T. Li**[3], **Weg M. Ongkeko**[3], **Ezra E.W. Cohen**[4,5], **J. Silvio Gutkind**[2,4], **Stephen R. Adams**[2], **Sunil J. Advani**[1,4,*]

[1]Department of Radiation Medicine and Applied Sciences, University of California San Diego, La Jolla, CA 92093

[2]Department of Pharmacology, University of California San Diego, La Jolla, CA 92093

[3]Division of Otolaryngology-Head and Neck Surgery, Department of Surgery, University of California San Diego, La Jolla, CA 92093

[4]UC San Diego, Moores Cancer Center, La Jolla, CA 92093

[5]Department of Medicine, Division of Hematology and Oncology, University of California San Diego, La Jolla, CA 92093

Abstract

Patients with advanced cancers are treated with combined radiotherapy and chemotherapy, however curability is poor and treatment side effects severe. Drugs sensitizing tumors to

[*]Corresponding Author Sunil J. Advani, Department of Radiation Medicine and Applied Sciences, Moores Cancer Center, University of California San Diego, 3855 Health Sciences Drive, MC 0843, La Jolla, CA 92093-0843, Phone: 858-822-6046, Fax: 858-822-5568, sjadvani@ucsd.edu.

[#]contributed equally

Credit author statement

Dina V. Hingorani: Investigation, Visualization, Writing- Original Draft.
Jessica L. Crisp: Investigation, Visualization.
Matthew K. Doan: Investigation.
Maria F. Camargo: Investigation.
Maryam A. Quraishi: Investigation.
Joseph Aguilera: Investigation.
Mara Gilardi: Investigation.
Larry A. Gross: Methodology, Investigation.
Tao Jiang: Methodology, Investigation.
Wei T. Li: Investigation.
Weg M. Ongkeko: Data Curation.
Ezra E.W. Cohen: Resources, Writing-Review & Editing.
J. Silvio Gutkind: Resources, Writing-Review & Editing.
Stephen R. Adams: Methodology, Resources, Writing-Review & Editing.
Sunil J. Advani: Conceptualization, Writing-Original Draft, Supervision, Funding acquisition.

Declaration of competing interests

University of California San Diego has filed patent applications based on the findings described in this manuscript (S.R.A. and S.J.A.). The remaining authors declare no competing financial interests.

Data availability

All of the data reported in this work are available upon reasonable request from the corresponding author.

radiotherapy have been developed to improve cell kill, but tumor specificity remains challenging. To achieve tumor selectivity of small molecule radiosensitizers, we tested as a strategy active tumor targeting using peptide-based drug conjugates. We attached an inhibitor of the DNA damage response to antibody or cell penetrating peptides. Antibody drug conjugates honed in on tumor overexpressed cell surface receptors with high specificity but lacked efficacy when conjugated to the DNA damage checkpoint kinase inhibitor AZD7762. As an alternative approach, we synthesized activatable cell penetrating peptide scaffolds that accumulated within tumors based on matrix metalloproteinase cleavage. While matrix metalloproteinases are integral to tumor progression, they have proven therapeutically elusive. We harnessed these pro-tumorigenic extracellular proteases to spatially guide radiosensitizer drug delivery using cleavable activatable cell penetrating peptides. Here, we tested the potential of these two drug delivery platforms targeting distinct tumor compartments in combination with radiotherapy and demonstrate the advantages of protease triggered cell penetrating peptide scaffolds over antibody drug conjugates to deliver small molecule amine radiosensitizers.

Graphical Abstract

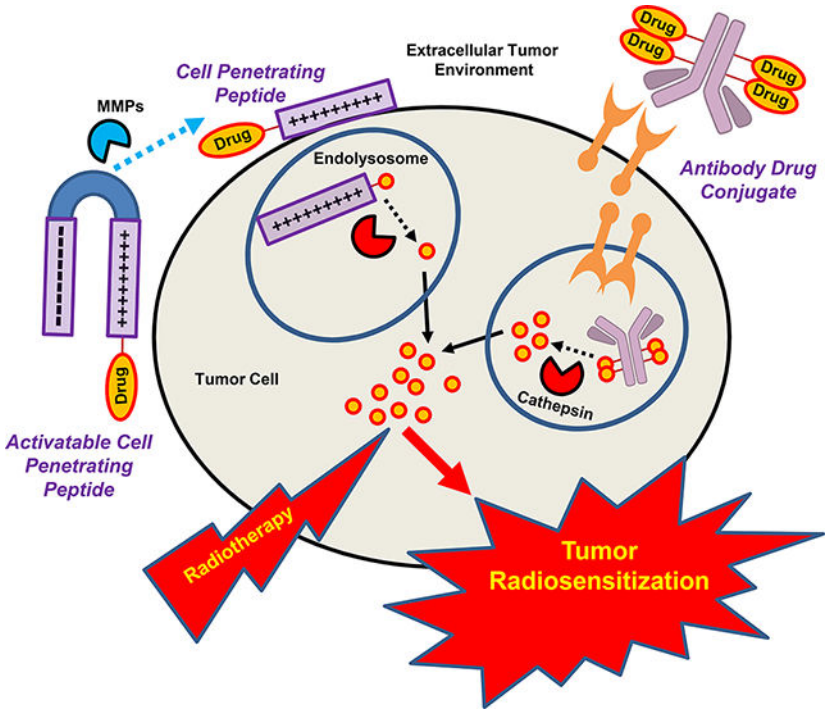

Keywords

Targeted drug delivery; Cell penetrating peptides; Antibody drug conjugates; Radiosensitization; Radiotherapy

Introduction

Locally advanced cancers that have not metastasized continue to pose a therapeutic challenge. The infiltrative nature of such cancers into surrounding normal tissue and

lymphatic spread precludes surgical curability. For such patients, randomized clinical trials have consistently demonstrated improved patient outcomes when radiotherapy is concomitantly given with chemotherapy [1–8]. Rationales for combining focally targeted ionizing radiation (IR) with systemically administered drugs include: 1) Spatial cooperativity of radiotherapy aimed at identifiable macroscopic tumor and chemotherapy simultaneously attacking subclinical microscopic cancer spread. 2) Independent mechanisms of tumor kill by chemotherapeutics and radiotherapy decrease the emergence of treatment resistant tumor clonogens. 3) Finally, a major motivation for concurrent chemo-radiotherapy is that certain drugs radiosensitize, i.e. increase IR induced DNA damage and tumor cell kill.

While radiotherapy delivery techniques have become increasingly sophisticated to incorporate advanced imaging inputs from CT, MRI and PET scanners to conform IR dose deposition to identifiable macroscopic disease, radiosensitizing drugs given with complex intensity modulated radiotherapy remain non-targeted broad spectrum chemotherapies (i.e. cisplatin, taxanes and 5-FU) [9–11]. Though such classical cytotoxic drugs improve tumor control, organ preservation and overall survival in combination with IR, they unfortunately increase normal tissue damage both in and out of the irradiated target zone [12]. Therefore, more precise tumor radiosensitization strategies are needed to increase the therapeutic ratio of radiotherapy [13–16]. Following IR, cell death primarily occurs through DNA double strand breaks resulting in chromosomal aberrations and ultimately clonogenic cell death. Mechanistic elucidation of cellular responses to IR has delineated key DNA damage response pathways [17]. Importantly, the DNA damage repair axis can be pharmacologically inhibited with readily available small molecule inhibitors. Though many radiosensitizers have been developed, a bottleneck in clinical translation is lack of tumor specificity. Non-targeted drugs sensitize not only tumor cells to IR, but also the surrounding normal tissue which essentially negates any widening of the therapeutic window in combination with radiotherapy.

To address this fundamental problem, we have focused on developing orthogonal approaches to tumor radiosensitization by splitting the responsibilities for tumor targeting and radiosensitization into two distinct molecular tasks [18–20]. In principle, such a strategy attaches a radiosensitizing drug to a delivery vehicle. The tumor and its microenvironment possess localizing beacons that can actively guide drug delivery and can be therapeutically exploited. These include tumor cell intrinsic surface receptors and tumor extracellular matrix metalloproteinases (MMPs). Clinically successful examples of such a paradigm include antibody drug conjugates (ADCs) [21–26]. ADCs consist of highly potent cytotoxic drug warheads attached to an antibody. Tumor selectivity is achieved by using antibodies recognizing membrane receptors overexpressed on tumor cells compared to normal tissue. Following antibody binding to the cell surface receptor antigen, the conjugated warhead drug payload is internalized and selectively kills tumor cells in a receptor restricted manner. Similar to ADCs, smaller cell penetrating peptides can be drug conjugated to facilitate tumor targeted drug delivery [18, 27, 28].

Here we applied protein and peptide drug delivery technologies to achieve tumor selective drug delivery and radiosensitization with AZD7762. AZD7762 is a small molecule inhibitor that governs DNA damage response and cell fate after IR [29, 30]. We synthesized drug

conjugates of AZD7762 and compared their anti-tumor efficacy in combination with IR. An ADC was built by attaching AZD7762 to the anti-EGFR antibody cetuximab. Polycationic cell penetrating peptide drug conjugates were constructed by linking AZD7762 to a 9 amino acid polypeptide repeat of D-arginine and keeping it bare or cloaking it within a MMP-2/9 targeted activatable cell penetrating peptide (ACPP) scaffold. In contrast to receptor targeting of ADCs, ACPPs redirect extracellular tumor microenvironment proteases to guide drug delivery. Intact, ACPPs are charge neutral and prevent the conjugated drug from entering cells. Upon cleavage by tumor overexpressed extracellular proteases, the ACPP scaffold releases drug conjugated polycationic peptide which is then internalized by cells. We found that while ADC has high affinity for tumors and prolonged blood circulation, antibody conjugated AZD7762 lacked efficacy. On the other extreme, naked polycationic cell penetrating peptide AZD7762 conjugates radiosensitized but lacked tumor specificity. In contrast, MMP-2/9 sensitive ACPPs balance tumor selectivity with drug efficacy. Intact, ACPPs held conjugated AZD7762 in a pro-drug inactive state that required tumor microenvironment cleavage for anti-tumor efficacy with IR. These results highlight the utility of the ACPP technology platform to target radiosensitizing drugs to tumor tissues based on extracellular protease activity.

Results

DNA damage response inhibitor AZD7762 is amenable to peptide conjugation

To evaluate the efficacy of tumor honing delivery platforms to deliver drugs that sensitize cancer cells to radiotherapy, we focused on AZD7762 as the drug payload since it has an amine group facilitating peptide attachment (Fig. 1A). Importantly, AZD7762 is a small molecule inhibitor of DNA damage checkpoint kinases CHK1 and CHK2 and increases IR induced cell death [29–31]. In a panel of cell lines from tumor histologies clinically treated with concurrent chemo-radiotherapy including head and neck, non-small cell lung, pancreatic and colo-rectal cancer, the potency of AZD7762 compared favorably to conventional cytotoxic chemotherapies routinely given together with radiotherapy (Fig. 1B). For drug conjugation, we first attached AZD7762 to a maleimidocaproyl-valine-citrulline-p-aminobenzyl carbamyl (MC-VC-PABC) linker which was subsequently attached to an antibody or a polycationic cell penetrating peptide (Fig. 1C) [32]. We selected the MC-VC-PABC linker since it is used in a clinically approved ADC, brentuximab vedotin [22]. After receptor mediated endocytosis of ADC, the valinecitrulline dipeptide within the MC-VC-PABC linker is cleaved by lysosomal cathepsin B which is then followed by self-immolation of the p-aminobenzyl carbomyl group to release the bound drug. To construct an ADC, AZD7762 was attached to the anti-EGFR antibody cetuximab through the MC-VCPABC linker (Supplemental Fig. 1). On average 4 AZD7762 molecules were loaded per antibody. For visual tracking, the ADC was labeled with Cy5. A concentration of 2 nM was used for Cy5 labeled cetuximab-AZ7762 based on our previous experience with imaging antibodies conjugated to auristatin warheads [19]. As expected, Cy5 tagged cetuximab-AZD7762 conjugate specifically bound EGFR expressing CAL27 cells but not to low EGFR expressing LN229 cells (Fig. 1D). As an alternative radiosensitizer delivery vehicle, we synthesized a polycationic cell penetrating peptide conjugate of AZD7762 by attaching it to a 9 amino acid repeat of D-arginine (r9-AZD7762) and similarly Cy5 labeled it

(Supplemental Fig. 2 and Supplemental Fig. 3). Cells were exposed to 100 nM Cy5 labeled r9-AZD7762 since 100 nM of free AZD7762 has been reported to radiosensitize [29, 30]. By fluorescent imaging, r9-AZD7762 conjugate was taken up indiscriminately by all tumor lines tested in cell culture (Fig. 1E).

Cell penetrating peptide conjugates of AZD7762 radiosensitize

Next, we tested the cytotoxicity of antibody and peptide conjugated AZD7762. For cetuximab- AZD7762, EGFR expressing CAL27 cells were assayed. As expected free AZD7762 produced dose dependent cell kill (Fig. 2A). However when conjugated to cetuximab, AZD7762 lacked cytotoxicity at a concentration of up to 3 uM. Evaluating higher doses of ADC was technically constrained by the limitation of antibody concentration achievable. As a positive ADC cytotoxic control, we conjugated cetuximab to an auristatin anti-tubulin, monomethyl auristatin E (MMAE). MMAE was highly potent at killing cells as either a free drug or as an antibody conjugate. This suggested that antibodies could not deliver a therapeutic concentration of the lower potency AZD7762. In contrast to lack of efficacy as an antibody conjugate, AZD7762 linked to r9 polycationic cell penetrating peptide demonstrated cell kill across cell lines albeit with decreased potency compared to free drug (Fig. 2B). PANC1 cells were a notable exception where the r9 conjugate had a similar IC_{50} to free AZD7762. Given that polycationic peptide conjugates of AZD7762 retained cytotoxicity, we tested their potential to sensitize tumor cells to ionizing radiation. As expected, free AZD7762 significantly increased irradiation induced cell death in clonogenic assays. Importantly, treating tumor cells with r9-AZD7762 also radiosensitized tumor cells as effectively as free drug (Fig. 2C).

Non-invasive tracking antibody and cell penetrating peptides in tumor bearing mice

While cell penetrating peptide conjugates of AZD7762 sensitized tumor cells to IR mediated kill *in vitro*, they inherently lack an active targeting mechanism for tumor specific delivery *in vivo*. To provide a tissue restricted delivery solution for polycationic cell penetrating peptides, we have developed protease activated cell penetrating peptides, ACPPs (Fig. 3A) [28, 33, 34]. ACPP is constructed with modular architecture and minimally consists of 3 domains: a polycationic cell penetrating peptide (nine repeats of D-arginine, r9), a polyanionic autoinhibitory domain (nine repeats of D-glutamic acid, e9), and an intervening flexible peptide linker (PLGC(Me)AG). For drug delivery, the drug payload is attached to the cell penetrating peptide domain of ACPP [18, 35]. While ACPP is intact, the bound drug is held in a “pro-drug” like inaccessible state due to charge neutralization of the polycationic cell penetrating peptide by the adjacent polyanionic peptide which blocks intracellular entry. Cleavage of the intervening linker within ACPP “triggers” it by removing the spatial proximity of the inhibitory polyanionic charge to the polycationic cell penetrating peptide. Since tumors are enriched in matrix metalloproteinases to promote invasive growth, ACPP tumor targeting can be achieved by inserting a MMP-2/9 sensitive PLGC(Me)AG peptide linker between the charged domains. Tumor microenvironment MMP-2/9 gelatinase activity cleaves ACPP and releases the r9 cell penetrating peptide-drug conjugate which then electrostatically adheres to cell membranes and is endocytosed.

To compare tumor distribution of systemically delivered antibody, polycationic cell penetrating peptides and ACPPs, we synthesized Cy5 fluorescently labeled cetuximab, r9 and ACPP probes (Fig. 3A). In our murine tumor models, we tested for differential tissue MMP-2/9 protease activity. Tumor and the adjacent muscle were harvested and assayed by gelatin zymography (Fig. 3B and Supplemental Fig. 4). Gelatinase activity was enriched in both CAL27 and PANC1 tumors compared to underlying muscle tissue. Cy5 labeled cetuximab, r9 and ACPP probes were tail vein injected into mice bearing bilateral thigh CAL27 tumors and visually tracked over the course of 48 hrs. (Fig 3C). Whole mouse imaging showed Cy5 fluorescence within the bilateral tumors with each probe. Control mice injected with water vehicle showed only gut autofluorescence and no tumor Cy5 signal (Supplemental Fig. 5A). Cetuximab antibody probe showed gradual increase in tumor Cy5 signal over 48 hrs. with minimal non-tumor Cy5 fluorescence. Cy5 labeled r9 showed quick increase in Cy5 signal in tumor and also the overlying skin. Cy5 labeled ACPP also had tumor rapid Cy5 signal in tumor, but appeared to have reduced non-tumor fluorescence.

ACPP scaffold spatially targets cell penetrating peptides to tumors

To interrogate normal tissue and tumor differential distribution of systemically delivered polycationic cell penetrating peptides with ACPPs we focused on further evaluating the injection site (tail vein) and intended target (tumor). Mice with bilateral thigh CAL27 tumors were intravenously injected through the tail vein with Cy5 labeled r9 and ACPP. Whole tail non-invasive imaging revealed that r9 probe produced a higher Cy5 signal in the tail compared to ACPP following intravenous tail vein injection (Fig. 4A and Supplemental Fig. 5B). At 90 minutes after peptide injection, tissues including tail, tumor and peri-tumoral muscle were harvested. Microscopy confirmed significantly higher Cy5 signal accumulation in the tail vein injection site from mice injected with r9 cell penetrating peptide as opposed to ACPP (Fig. 4B). Next the target tumor and adjacent muscle were identified by H&E staining on harvested tissue (Fig. 4C). While both the r9 or ACPP probes produced Cy5 fluorescence within tumors, the ratio of Cy5 signal in tumor to adjacent muscle was significantly higher in mice injected with ACPP probe compared to naked r9 (Fig. 4D). Taken together, these results provide evidence that the ACPP scaffold can widen the therapeutic index of conjugated drugs by selectively targeting polycationic cell penetrating peptides to tumors and avoiding normal tissues.

In situ cleavage of ACPP marks tumors

To determine the applicability of PLGC(Me)AG guided ACPP drug delivery, we assayed MMP-2/9 gelatinase activity in patient tumor tissue samples from histologies routinely treated with combined chemotherapy and radiotherapy. Tumors collected from head and neck, lung, colorectal and pancreatic cancer patients all possessed gelatinase activity (Fig. 5A). Clinically, tumor MMP expression has been correlated with advanced tumor stage and poor prognosis [36]. In a TCGA based analysis of HNC patients, we also found that MMP-2/9 expression correlated with a poor prognostic marker associated with decreased local-regional tumor control, perineural tumor invasion (Fig. 5B). Next, we determined if ACPP were cleaved *in situ* by human tumors. Ratiometric ACPP was synthesized by attaching a Cy5 far red fluorescent donor the polycationic cell penetrating peptide and a Cy7 near infrared fluorescent acceptor to the polyanionic peptide (Fig. 5C) [37]. First, we

directly confirmed that ratiometric ACPP was cleaved by incubating it with recombinant MMP-9 and measuring remaining intact ratiometric ACPP (Fig 5D).

While ratiometric ACPP is intact, Cy7 re-emission is favored when excited with Cy5 excitation wavelengths, resulting in a low Cy5:Cy7 emission ratio (blue pseudocolor). However if the peptide linker is cleaved, Cy5 emission is no longer quenched and Cy5:Cy7 emission ratio increases (red pseudocolor). Mice with subcutaneous GFP expressing CAL27 tumors were injected with ratiometric ACPP containing a non-cleavable polyethylene glycol (PEG) linker or MMP-2/9 cleavable PLGC(Me)AG peptide linker. Increased Cy5:Cy7 emission ratio was found in tumors from mice injected with the cleavable PLGC(Me)AG ACPP (Fig. 5E and Supplemental Fig. 6A). Mice injected with the non-cleavable PEG ACPP had a low Cy5:Cy7 emission ratio confirming the necessity of cleavage of ratiometric ACPP for signal alteration. Advancing to orthotopic tongue tumors, CAL27 tumor bearing tongue tips also had increased ratiometric ACPP cleavage compared to adjacent non-cancerous tongue muscle (Fig. 5F and Supplemental Fig. 6B). Finally, we queried if ratiometric ACPP was cleaved directly in a patient tumor biopsy. As seen with human tumor xenografts, ratiometric ACPP with cleavable PLGC(Me)AG linker had elevated Cy:5:Cy7 emission ratio in patient biopsy specimen (Fig. 5G). These results demonstrate that ACPP probes with a PLGC(Me)AG linker can harness extracellular tumor microenvironment proteases to demarcate tumor tissue and actively target polycationic cell penetrating peptides to tumors.

ACPP targeted AZD7762 improves irradiated tumor control

Finally, we evaluated the efficacy of ACPP conjugated AZD7762 in combination with IR in murine models. We attached MC-VC-PABC-AZD7762 to the r9 cell penetrating peptide portion of ACPP by maleimide reaction with a C-terminal cysteine followed by modification of the N-terminal amine with an integrin-targeting cRGD active ester (Fig. 6A) [35]. The high specificity of these reagents limit side reaction with additional ACPP domains and therefore protection of carboxylic and amine/guanidine groups was not needed. The cleavage of ACPP-AZD7762 was measured by incubating the synthesized peptide drug conjugate with recombinant MMP-9 (Fig. 6B). To test the efficacy of peptide drug conjugate based radiosensitization, mice bearing CAL27 tumors were intravenously injected with a single dose of AZD7762 as free drug, r9 conjugate or ACPP conjugate (Fig. 6C). For drug conjugated ACPP, we included a co-targeting cRGD on the ACPP scaffold since tumor expressed $\alpha v\beta 3$ integrins promote MMP-2/9 activity (Supplemental Fig. 2 and Supplemental Fig. 7) [35, 38]. IR was given focally to the tumor bearing hindlimbs with the remainder of the mouse shielded. Combining ACPP-AZD7762 and IR produced significant delayed tumor growth compared to all other treatment groups by day 14. Importantly in mice receiving IR, only the addition of ACPP-AZD7762 resulted in tumor growth delay while free AZD7762 or r9-AZD7762 did not. To optimize scheduling of ACPP drug delivery with IR, we evaluated the blood clearance of ACPP. Cy5 labeled ACPP was intravenously injected and Cy5 signal in blood serially measured (Fig. 6D). After an initial elevation of blood Cy5 fluorescence immediately following intravenous injection, ACPP blood concentration rapidly fell and was approximately 5% of maximum signal intensity at 90 minutes post injection. ACPP blood clearance is in stark contrast to the persistence of

antibody, where blood levels of cetuximab remained at 33% of maximum at 24–48 hrs. post injection (Supplemental Fig. 8).

To corroborate our fluorescent peptide probe findings, we directly measured tissue AZD7762 levels following ACPP drug conjugate injection. Mice bearing CAL27 tumors were intravenously injected with ACPP-AZD7762 and blood and tissues were assayed for drug. At 2 hrs. post, AZD7762 concentration was 4.8 fold higher in tumors compared to adjacent non-cancerous muscle tissue (Fig. 6E). Drug accumulation in peri-tumoral muscle was minimal and essentially equivalent to that of circulating blood. Interestingly, ACPP-AZD7762 conjugate had quick wash out kinetics from tumors. By 16 hrs., drug concentration in tumor decreased to levels found in blood. Since our initial results showed that only ACPP-AZD7762 increased tumor control of irradiated tumors compared to free drug or r9 conjugate, we next tested the necessity of ACPP peptide linker to improve tumor control in combination with ionizing radiation. We attached AZD7762 to an ACPP with a D-amino acid linker, plGc(Me)aG and cRAD scaffold (d-ACPP-AZD7762) (Supplemental Fig. 3). Mice with PANC1 tumor xenografts treated with combined IR and the cRGD and L-amino acid linker ACPP drug conjugate demonstrated significant growth delay (Fig. 6F and Supplemental Table 1). In contrast, AZD7762 conjugated to a ACPP with a D-amino acid linker and cRAD did not provide any additional tumor control to IR alone. Given the rapid decrease of intratumoral AZD7762 concentration (Fig. 6E), we tested a dose intense combination of ACPP-AZD7762 and IR to improve tumor control. While repeated daily injections of ACPP-AZD7762 or fractionated ionizing radiation alone were ineffective, the combination of ACPP-AZD7762 with daily IR significantly increased survival of CAL27 tumor bearing mouse (Fig. 6G and Supplemental Table 2). Equally important, the combination of ACPP conjugated AZD7762 and irradiation did not adversely affect mouse well-being (Supplemental Fig. 9).

Discussion

The modular architecture of peptide-based drug conjugate chemistry allowed us to directly compare different active tumor targeting approaches for radiosensitizers, i.e. ADC using intrinsic tumor cell surface receptors or ACPP using extracellular tumor microenvironment proteases. ADCs are highly precise due to specificity of the targeting antibody for cell surface receptors overexpressed on certain tumors. To this point, fluorescently labeled delivery vehicle tracking revealed that cetuximab had minimal Cy5 signal at the initial tail vein injection site compared to r9 cell penetrating peptide or ACPP (Fig. 3C and Supplemental Fig. 5B). Unfortunately, ADCs have had limited oncologic applications to date. A major weakness is that only a few cell surface receptors have been identified that are overexpressed specifically on tumors and can be therapeutically exploited [11]. Targeting HER2+ breast cancer with trastuzumab emtansine (T-DM1) is the sole successful translation of ADCs for solid cancers [23]. For purer radiosensitization applications, ADC delivery has another major disadvantage secondary to cell receptor uptake limiting intracellular therapeutic drug levels. All successful examples of ADCs have been constructed using highly potent cytotoxic drug warheads with IC_{50} in the single nanomolar range that target essential cellular functions. Unfortunately, inhibitors of the DNA damage pathways are not as cytotoxic or potent as warheads used in clinically approved ADCs. Our synthesized

cetuximab-AZD7762 conjugate exposed this glaring ADC weakness. While cetuximab conjugated to AZD7762 bound specifically to EGFR expressing cells, it lacked cytotoxicity seen with a MMAE conjugate (Fig. 2A).

In contrast to ineffectiveness as an antibody conjugate, AZD7762 attached to a polycationic cell penetrating polypeptide remained cytotoxic and radiosensitized (Fig. 2B and Fig. 2C). Cell penetrating peptide drug delivery is not receptor density limited. Therefore, less potent radiosensitizing drugs can achieve effective intracellular concentrations. However, polycationic cell penetrating peptides inherently lack tumor specificity. To provide an active targeting mechanism for polycationic cell penetrating peptides, we integrated the drug conjugated r9 peptide into an ACPP scaffold (Fig. 3A). ACPPs depend on MMPs to cleave the intervening linker peptide which removes charge neutralization and allows intracellular uptake of drug bound cell penetrating peptide. Importantly, MMPs play fundamental roles in cancer progression which have made them attractive targets for pharmacologic blockade [39]. While MMP inhibitors have been successfully developed, they failed to have clinical benefit. Given the lack of therapeutic success for enzyme inhibition, an alternative anti-cancer strategy is redirecting MMP enzymatic protease activity for therapeutic gain. This was a primary motivation in designing ACPPs. From a therapeutic ratio, ACPPs had decreased normal tissue accumulation and increased tumor specificity compared to cell penetrating peptides (Fig. 4). Importantly in combination with ionizing radiation, ACPP drug conjugation improved tumor control compared to either free drug or r9 cell penetrating peptide conjugate (Fig. 6C). This suggests active tumor targeting by ACPPs can improve the therapeutic index of radiotherapy of not only free drug but also non-targeted cell penetrating peptides.

Our results with fluorescently labeled delivery vehicles highlight important pharmacodynamic differences between ADC and ACPP platforms to optimize sequencing with IR. In prior studies with anti-tubulin ADCs, a single dose of ADC resulted in drug detectable within tumors for 3 days and single dose of ADC in combination with daily IR produced tumor control [19, 20]. In contrast, ACPP blood clearance is much quicker than ADC which correlated to a shorter window of tumor AZD7762 accumulation (Fig. 6D, Fig. 6E and Supplemental Fig. 8). This has implications in optimizing the sequencing ACPP drug conjugates with IR. Clinically, IR is delivered daily for multiple days. DNA damage occurs almost instantaneously after irradiation. Given the rapid excretion of ACPP from the circulation, ACPP drug delivery can be more adeptly tuned to maximize tumor kill in the irradiated target than ADCs. To this point, we found that giving ACPP daily with IR produced sustained tumor control (Fig. 6G). Moreover, ACPPs are also much smaller than ADCs which can facilitate improved tumor penetration.

The modular design of ACPPs allows them to function as biosensors to evaluate tissue microenvironment processes *in situ*. Ratiometric labeled ACPP molecular probes non-invasively monitor tumor extracellular protease activities to provide information on tumor microenvironment evolution how it is influenced by anti-cancer therapies [40]. Interestingly, MMPs are induced by IR and modulate tumor response to IR [40–44]. Moreover, IR has been shown to increase macromolecule delivery to the irradiated target independent of endothelial cell integrity [45]. This suggests ACPPs can interrogate and therapeutically

exploit irradiated tumor microenvironments. While we focused on MMP-2/9 sensitive PLGC(Me)AG linker, other peptide linker sequences can be incorporated between the charged peptide domains of ACPP to characterize and harness the interplay of different classes of tumor microenvironment extracellular proteases on tumor progression. Interestingly, other tumor targeting peptides are being developed to target irradiated tumors such as Tax-interacting protein-1 (TIP-1) [46, 47].

In summary, our ACPPs leverage MMP protease activity for enzymatic directed drug delivery of radiosensitizer conjugated cell penetrating peptides. Tumor targeted peptide-based radiosensitizer drug delivery has the potential to spatially and temporally cooperate with radiotherapy to improve tumor kill while reducing normal tissue toxicity. Harnessing tumor microenvironment extracellular proteases, ACPPs function as molecular probes to mark tumor regions and can selectively deliver their drug conjugated radiosensitizer payload into tumor regions associated with poor prognosis. Importantly, the ACPP platform offers solutions to the limitations posed by ADCs for delivering less potent radiosensitizing warheads. Given structural requirements, our initial studies evaluated commercially available AZD7762 conjugates due to the presence of an amine group facilitating linkage to antibody or ACPP. However, other inhibitors of the DNA damage response may be amenable to peptide conjugation especially as linker chemistry advances.

Materials and Methods

Cells and Reagents

Human head and neck CAL27, lung A549, pancreatic PANC1, colorectal HCT116 and glioma LN229 cancer cell lines were obtained from American Type Culture Collection. CAL27, A549, HCT116, PANC1 cells and LN229 were cultured in DMEM supplemented with 10% FBS. On initial receipt, cell lines were expanded and low passage stocks cryopreserved without further authentication testing. Cells were passaged 2 times per week and used for 4–6 weeks after which a new stock vial was thawed. Cells were routinely tested for mycoplasma by PCR, and testing was performed prior to cell implantation in mice for xenograft experiments. AZD7762 (Selleck Chemicals) was reconstituted in dimethyl sulfoxide (DMSO). Clinical grade cetuximab was obtained from UCSD Moores Cancer Center pharmacy.

Synthesis of antibody drug conjugate

A solution of cetuximab (1 ml, 2 mg/ml, 15.7 nmol; measured at A_{280} with an extinction coefficient of 211,370 $M^{-1}cm^{-1}$) was treated with bicine buffer (1 M, 100 μl, pH 8.3) and Na_2DTPA (100 mM, 10 μl) and reduced at 37°C for 2 hrs. by the addition of TCEP (10 mM, 6.3 μL, 63 nmol). After cooling to room temp., MC-VC-PABC-AZD7762 (74 μl of a 0.85 mM solution in DMSO, 63 nmol, mixed with 74 μl of water immediately before addition; synthesis described below) was added for 1 hr. followed by Cy5maleimide (31 μl of a 1 mM solution in DMSO, 31 μmol, mixed with 31 μl of water immediately before addition) for a further 1 hr. The reaction mixture was passed through a column of Sephadex G-25 (1 g in PBS) collecting the first blue-colored band and concentrated with a 30kD MWCO spin-filter (Centricon) to ~0.5 mL. Absorbance measurements (in PBS) indicated an average of 4 MC-

VC-PABCAZD7762 and 1.1 Cy5 were attached to cetuximab using extinction coefficients of Cy5 at 650, 310 and 280 nm of 250000, 10750 and 12500 $M^{-1}cm^{-1}$ respectively, and extinction coefficients of MC-VC-PABCAZD7762 at 310 and 280 nm of 15000 and 11100 $M^{-1}cm^{-1}$ respectively. Analysis by HILIC and denaturing LC-MS revealed the expected mixture of conjugates (Supplemental Fig. 1). Cetuximab conjugated monomethyl auristatin E was synthesized as previously described [19].

Synthesis of drug conjugated cell penetrating peptides

General synthetic schema and chemical structures of peptide conjugates used are shown in Supplemental Fig. 2 and Supplemental Fig. 3. To attach AZD7762 to the maleimidocaproyl-valinecitrulline-p-aminobenzyl carbamyl linker (MC-VC-PABC), a solution of AZD7762 free base (10 mg, 27.5 μmol) in dry DMSO (100 μl) was mixed with a solution of MC-VC-PABC-PNP (Synchem; 80%, 28 mg, 30.3 μmol in dry DMSO (100 μl) and N-methylmorpholine (NMM) (3.3 μL, 30.3 μmol) was added. The reaction was complete within 15 minutes at room temperature by LC-MS and quenched with acetic acid (5 μl), separated by HPLC (acetonitrile (ACN)-water-0.05% trifluoroacetic acid (TFA)) and lyophilized to a white powder. Yield was 11.2 μmol of MC-VC-PABC-AZD7762 TFA salt (yield 41%). By ES-MS, observed mass 961.2 ($M+H^+$) and calculated for $C_{46}H_{57}FN_{10}O_{10}S$, 961.40. Extinction coefficient at 310 nm = 15000 $M^{-1}cm^{-1}$. To synthesize Cy5 labeled r_9-MC-VC-PABC-AZD7762, H_2N-r_9-c-$CONH_2$ 10·TFA (6.3 mg, 2.4 μmol) dissolved in 200 μl of ACN-water-TFA (50:50:0.05%) was reacted with a solution of MC-VC-PABC-AZD7762 (2.3 mg, 2.4 μmol) in 200 μl of DMSO and 100 μL of 1M Na·MOPS pH 7.2 at room temperature. LC-MS revealed the reaction was complete in 15 min, and then was quenched with 50 μL acetic acid (HOAc), separated by HPLC and lyophilized to give H_2N-r_9-c- MC-VC-PABCAZD7762 as a white powder. ES-MS, fnd 622.7 ($M+3H^+$), 829.8 ($M+2H^+$) deconvolved to 2486.5, calculated for $C_{103}H_{173}FN_{48}O_20S_2$, 2486.3. H_2N-r_9-c- MC-VC-PABC-AZD7762 (4.5 mg, 1.25 μmol as salt with 10·TFA) was dissolved in dry DMSO (200 μL) and mixed with a solution of Cy5-NHS ester (1.1 mg, 1.5 μmol) and NMM (2 μL, 20 μmol) were added. After 1 week at room temperature, the product was isolated by HPLC and lyophilized to a blue powder. By ES-MS, observed mass 782.4 (M^++$3H^+$), 1042.7 (M^+ +$2H^+$), 1563.7 (M^++H^+) deconvolved to 3125.3, calculated for $C_{136}H_{212}FN_{50}O_{27}S_4^+$, 3124.6. To synthesize cRGD-*L*-ACPP-AZD7762, H_2N-peg8-e_9-oPLGC(Me)AG-r_9-c-$CONH_2$ was made using regular solid phase Fmoc peptide synthesis, where lower case letters refers to D-amino acids, peg8 refers to H_2N-PEG8-propionic acid (Quanta BioDesign), o-denotes for 5-amino-3-oxopentanoyl a short hydrophilic spacer, C(Me) denotes for S-methylcysteine and the final $CONH_2$ indicates C-terminal amide. The peptide was isolated from the resin by treating it with mixtures containing 92% TFA, 2% thioanisole, 2% water, 2% ethanedithiol and 2% triisopropylsilane (TIPS) for 4 hrs. under N_2 atmosphere and filtered. This filtrate was concentrated and then precipitated by addition of ice cold 50% hexanes in ethyl acetate mixture. The precipitate was collected by centrifugation and dried under vacuum. The crude peptide was dissolved in DMSO and purified by high performance liquid chromatography (HPLC) using 5–55% acetonitrile in water and 0.05% TFA over a period of 25 minutes at 15 mL per min flow rate. The purified product was dried using lyophilization. By ES-MS, observed mass of 621.4 (M^++$6H^+$), 745.8 (M^++$5H^+$), 932.0 (M^++$4H^+$), 1242.4 (M^++$3H^+$), deconvolved to 3724.9 (M^++H^+),

calculated for $C_{147}H_{259}N_{55}O_{54}S_2$, 3723.87. H_2N-peg8-e_9-oPLGC(Me)AG-r_9-c-$CONH_2$ (10·TFA salt, 73 mg, 15 μmol) dissolved in dry DMSO (100 μL) was reacted with crude MC-VC-PABC-AZD7762 (prepared from AZD7762 free base (5 mg, 13.8 μmol) in dry DMSO (50 μl) reacted with a solution of MC-VC-PABC-PNP (Synchem; 80%, 14 mg, 15.1 μmol in dry DMSO (50 μl) and NMM (1.5 μL, 15 μmol) for 30 min). NMM (10 μL, 100 μmol) was added and LC-MS indicated complete reaction after 30 minutes to give a single product that was used without further purification. ES-MS observed mass of 782.1 (M^++6H^+), 938.2 (M^++5H^+), 1172.5 (M^++4H^+), 1562.9 (M^++3H^+), deconvolved to 4687.0 (M^++H^+), calculated for $C_{193}H_{316}FN_{65}O_{64}S_3$, 4687. Cyclo(RGDfC) (Peptides International; 8.7 mg, 15 μmol) dissolved in dry DMSO(50 μL) was mixed with a solution of 6-maleimidocaproic acid (2-nitro-4sulfo)phenyl ester (Bachem; 5.9 mg, 13.5 μmol) in dry DMSO (50 μL) and NMM (3.3 μL, 30 μmol). LC-MS indicated complete reaction after 30 minutes to yield the adduct, ES-MS observed 991.4 (M^++H^+), calculated for $C_{40}H_{50}N_{10}O_{16}S_2$, 991.28. This crude product was added to the reaction mix of H_2N-peg8e_9-oPLGC(Me)AG-r_9-c-(MC-VC-PABC-AZD7762)-$CONH_2$ prepared above and kept at room temperature until complete by LC-MS (1–2 weeks), and then was quenched with HOAc (50 μL), separated by HPLC and lyophilized to give cyclo(RGD)fc-MC-HN-peg8-e_9-oPLGC(Me)AG-r_9-c-(MC-VCPABC-AZD7762)-$CONH_2$ = cRGD-*L*-ACPP-AZD7762, a white powder with a yield of 32.9 mg (34%). By ES-MS observed mass 780.81 (M^++7H^+), 910.7 (M^++6H^+), 1092.6 (M^++5H^+), 1365.4 (M^++4H^+), deconvolved to 5458.8 (M^++H^+), calculated for $C_{227}H_{361}FN_{74}O_{74}S_4$, 5459.07. To synthesize cRAD-*D*ACPP-AZD7762, it was prepared as above for cRGD-*L*-ACPP-AZD7762 but using H_2N-peg8-$e_9$oplGc(Me)aG-r_9-c-$CONH_2$ and cyclo(RADfC) to give the product as a white powder and yield of 63%. By ES-MS observed mass 912.8 (M^++6H^+), 1095.2 (M^++5H^+), 1368.7 (M^++4H^+), 1824.5 (M^++3H^+), deconvolved to 5471.6 (M^++H^+), calculated for $C_{228}H_{363}FN_{74}O_{74}S_4$, 5473.03.

Alamar Blue assay

Cells were plated in 96 well plates and exposed to a concentration range of AZD7762, cisplatin, 5fluorouroacil (5-FU), cetuximab, cetuximab conjugated AZD7762, r9 alone or r9 conjugated to AZD7762 (r9-AZD7762) for 72 hrs. Alamar Blue was added to the cells and allowed to incubate for 2–4 hrs. at 37°C. Plates were analyzed using a plate reader with fluorescence measured at 560 nm. Fractional survival was normalized to untreated control cell fluorescent values. Drug IC_{50} was calculated using Prism software (GraphPad, La Jolla, CA).

In vitro Cy5 fluorescence imaging

Attached cells were exposed to 2 nM Cy5 labeled cetuximab-AZD7762 or 100 nM Cy5 labeled r9AZ7762 for 1 hr. in media containing 1% serum. Cells were then washed with PBS, fixed in 4% paraformaldehyde and stained with DAPI. Cells were imaged for Cy5 and DAPI signal using Nikon A1R confocal or Keyence BZX-710 fluorescence microscopes.

Clonogenic assay

Cells were treated with AZD7762, r9 alone or r9-AZD7762 conjugate for 1 hr. and then irradiated with 2 Gy. Cells were counted, re-plated at varying cell numbers in drug free media. After 10–14 days, cells were methanol fixed, stained with crystal violet and colonies

with at least 50 cells counted as viable. Surviving fraction at 2 Gy (SF2) was calculated as the number of colonies formed after 2 Gy divided by the number of colonies formed in non-irradiated groups for each drug condition.

Gelatin zymography assays

All animal work was done in compliance with the University of California San Diego Institutional Animal Care and Use Committee. 6–8 week old female athymic nu/nu mice (University of California San Diego Animal Care Program) were injected subcutaneously with 5 million CAL27 or PANC1 cells in 100 μl of 1:1 Matrigel (BD) and PBS solution. When tumors were palpable, tumor and peri-tumoral muscle were harvested and frozen in liquid nitrogen. For patient derived tissues, de-identified fresh frozen patient tumor samples (UCSD Moores Cancer Center Biorepository) were thawed on ice, cut into smaller pieces and placed in cold NP-40 lysis buffer containing both phosphatase and protease inhibitors. Samples were homogenized by passing through a syringe, centrifuged at 16,000g for 10min at 4°C, supernatants collected and protein concentration measured. 2x Tris Glycine SDS Sample Buffer was added to the samples and equivalent amounts of total protein loaded onto 10% zymogram gelatin gels (ThermoFisher). Gels were developed using Novex zymogram renaturing and developing buffers (10X) and stained with SimplyBlue Safestain (ThermoFisher). Purified MMP-2 and MMP-9 controls were loaded and run to identify locations of gelatinase activity.

Drug delivery vehicle distribution and blood clearance

Mice with established subcutaneous CAL27 tumors were anesthetized with isoflurane and intravenously injected through the tail vein with Cy5 labeled drug delivery peptides: 10 nanomoles r9, 10 nanomoles ACPP or 5 nanomoles cetuximab. For *in situ* detection of Cy5 signal, mice were imaged at indicated time points in the **Results** using a Maestro Small Animal Imager (CRI) with excitation filter of 620/22 nm and 685/40 nm pass emission filter with dichroic filter tuned to 670 nm and 150 ms exposure time. Tissue were then harvested at indicated time points, sectioned and stained with DAPI or H&E. H&E staining was used to demarcate tumor and adjacent normal muscle tissue. Cy5 fluorescence images were taken using the 640 nm laser line on a Nikon A1 confocal microscope with 20X/0.75 objective (tail) and 4X/0.20 objective (tumor and peri-tumoral muscle tissues). For blood clearance studies, the tail was pricked at indicated time points after injection, and a small volume (5–10μL) of blood was collected in a heparinized hematocrit tube. Fluorescent images were taken using the Maestro with filters mentioned above with 200 ms exposure time, and integrated fluorescent intensity quantitated using Image J software.

MMP and perineural invasions association in cancer patients

Level 3 normalized mRNA expression read counts for tumor samples from 500 head and neck squamous cell cancer patients and corresponding patient clinical data were downloaded on 14 July 2017 from The Cancer Genome Atlas (TCGA) (https://tcga-data.nci.nih.gov/tcga). 350 HNSCC patients had documented perineural invasion status, for which “Yes” was recorded if perineural invasion is present and “No” was recorded if it is absent. MMP-2 and MMP-9 gene expressions were correlated with perineural invasion status using the Kruskal-

Wallis test (p<0.05). To improve readability of the boxplot representations, 3 outliers were removed from the plot of MMP-2 expression vs. perineural invasion status, and 14 from the plot of MMP-9 expression vs. perineural invasion status, using the quartile method for data selection [48]. Expression values were removed if they lie above or below 3 times the interquartile range (IQR) from the median, which are considered extreme outliers. Moderate outliers, which lie above or below 1.5 times the IQR, were retained and plotted as dots above or below the plot whiskers.

In vitro cleavage of activatable cell penetrating peptides

Ratiometric ACPP were synthesized by attaching Cy5 to the polycationic cell penetrating peptide and Cy7 to the polyanionic peptide domains of ACPP as above [37]. A 1 ml solution of ratiometric ACPP (2.5 μM) or ACPP-AZD7762 conjugate (1 μM) was prepared in MMP buffer pH 7.4 (50mM Tris, 50mM NaCl, 10mM CaCl2, 10% glycerol). 0.5 μg of human recombinant MMP-9 (CalBioChem) was added. Samples were collected at time points indicated in **Results** and the reaction quenched with 1μl acetic acid. Samples were analyzed by LC-MS (95:5 Water+0.05% TFA: ACN +0.05% TFA to 50:50 Water+0.05% TFA: ACN +0.05% TFA) using Luna-2 C18 column.

Optical imaging of fluorescently labeled ratiometric ACPP

GFP expressing CAL27 tumor cells were subcutaneously implanted into athymic nude mice. After tumors developed, mice were anesthetized (1:1 mixture of 100 mg/ml of ketamine and 5 mg/ml of midazolam) and intravenously injected through the tail vein with Cy5 and Cy7 fluorescently labeled ratiometric ACPP containing a non-cleavable PEG linker or MMP-2/9 sensitive PLGC(Me)AG linker. For is situ detection, mice were imaged at 2 hrs. using a Maestro Small Animal Imager (CRI) with excitation filter of 620/22 nm and 645 nm long pass emission filter with dichroic filter tuned to 670 nm. For orthotopic murine tumors, 1×10^6 CAL27 tumor cells were submucosally implanted in the tongue of athymic nude mice. After tumors were palpable, 10 nmoles of ratiometric ACPP was intravenously injected in 100 μl of sterile water by tail vein injection. Tongues were imaged in situ and then harvested and imaged for Cy5 and Cy7 fluorescence. Tongues were longitudinally sectioned, stained for H&E, cytokeratin 5 (CK5) or β3 integrin (β3). Sectioned tissue was also directly imaged for Cy5 and Cy7 fluorescence. For frozen patient tumor biopsy specimens, tissues were snap frozen in OCT, 10 μm sections cut using a Lyca CM1950 cryostat and sections mounted on Trubond360 microscope slides (TruScientific). Immediately after cutting, tumor sections were incubated with 10 μM ratiometric ACPP in 0.5xHBSS (Gibco) for 30 minutes at 37°C. Slides were then imaged on a Nikon A1 laser confocal microscope using a 20X/0.75 Apo dipping objective with an excitation of 640 nm and collecting images at emission wavelengths of 685/50nm and 785/62 for Cy5 and Cy7 respectively. Image processing was done using Nikon NIS Elements software version 4.50 and Cy5:Cy7 ratiometric images generated using a custom image processing software.

In vivo tumor xenograft response experiments

CAL27 and PANC1 tumor xenografts were established and tumor growth measured using digital calipers. Tumor volumes was calculated using the formula as ½ * length * width^2.

Mice were randomly assigned to indicated groups in **Results**. Free AZD7762, r9-AZD7762 or ACPP-AZD7762 were i.v. injected in 50 μl. For irradiated mice, the tumor bearing hindlimbs were focally irradiated while the remainder of the mouse was shielded from IR with custom designed lead blocking > 95% of the dose as verified by dosimeters placed on the mouse. Drug doses and IR fractionation are indicated in **Results**. To minimize morbidity, mice were sacrificed if tumor length exceeded 15 mm per protocol. To minimize the number of mice used, tumors were grown in bilateral flanks. For CAL27 tumor xenograft experiment in Figure 6C, the average tumor volume per group was > 130 mm^3 and the number of mice and tumors per group were: Control (5 mice, 9 tumors), IR (5 mice, 10 tumors), AZD7762 (5 mice, 10 tumors), AZD7762 + IR (5 mice, 10 tumors), r9-AZD7762 (3 mice, 6 tumors), r9-AZD7762 + IR (3 mice, 6 tumors), ACPP-AZD7762 (5 mice, 10 tumors), ACPP-AZD7762 + IR (5 mice, 10 tumors). For PANC1 tumor xenograft experiment in Figure 6F, the average tumor volume per group was > 140 mm^3 and the number of mice and tumors per group were: Control (5 mice, 10 tumors), IR (5 mice, 10 tumors), dACPP-AZD7762 (5 mice, 10 tumors), d-ACPP-AZD7762 + IR (4 mice, 8 tumors), ACPP-AZD7762 (5 mice, 10 tumors), ACPP-AZD7762 + IR (5 mice, 10 tumors). For CAL27 tumor xenograft experiment in Figure 6G, the average tumor volume per group was > 110 mm^3 and the number of mice and tumors per group were: Control (5 mice, 10 tumors), IR (5 mice, 10 tumors), ACPP-AZD7762 (5 mice, 10 tumors), ACPP-AZD7762 + IR (5 mice, 10 tumors).

Tissue drug concentration

CAL27 tumor bearing mice were tail vein injected with ACPP-AZD7762 and tissues harvested at time points indicated in **Results**. Blood, tumor or peri-tumoral muscle were excised, weighed and homogenized in 10-volumes of PBS with a point sonicator (Fisher Scientific) using an amplitude range of 5% to 15% for a maximum of 20 seconds while on ice. Tissue homogenates were centrifuged (14g, 10min), supernatants collected and diluted two-fold by addition of 2% acetic acid in acetonitrile, and recentrifuged (14g, 10min). AZD7762 concentration was determined by LC-MS/MS with Luna-2 C18 column and Agilent Trap XCT mass spectrometer. To determine AZD7762 tissue concentrations, ion currents for m/z 346.1 and 320.14 were extracted from fragmented m/z 363.0 and m/z 368.0 and 342.1 were extracted from fragmented m/z 385.0. The ion currents were integrated and combined to improve sensitivity. The total ion current was fit to a standard curve generated to determine tissue drug concentration.

Statistical analysis

Unpaired 2-sided t tests or ANOVA with multiple comparisons were performed for experiments in cell culture. For murine tumor regression studies, 1-way ANOVA analysis (Fig. 6C) or 2way ANOVA analysis with Tukey’s multiple comparison group (Fig. 6F) were performed. Survival curves (Fig. 6G) were analyzed by Log-rank testing. All statistical analyses were done using Prism software (GraphPad, La Jolla, CA). Statistical analysis for tumor xenograft data are presented in Supplemental Table 1 and Supplemental Table 2.

Supplementary Material

Refer to Web version on PubMed Central for supplementary material.

Acknowledgements

This work is dedicated to Dr. Roger Y. Tsien, who intellectually nurtured the inception of this project and provided guidance in its initial stages. The authors thank Kersi Pestonjamasp for excellent technical assistance. This work was supported by the National Institutes of Health / National Cancer Institute CA205765 (SJA), CA215081 (SJA), CA219744 (SJA), P30CA23100 (Microscopy Core) and University of California Cancer Research Coordinating Committee CRR-17-422691 (SJA).

References

[1]. G. Department of Veterans Affairs Laryngeal Cancer Study, Wolf GT, Fisher SG, Hong WK, Hillman R, Spaulding M, Laramore GE, Endicott JW, McClatchey K, Henderson WG, Induction chemotherapy plus radiation compared with surgery plus radiation in patients with advanced laryngeal cancer, N Engl J Med 324(24) (1991) 1685–90. [PubMed: 2034244]

[2]. Adelstein DJ, Lavertu P, Saxton JP, Secic M, Wood BG, Wanamaker JR, Eliachar I, Strome M, Larto MA, Mature results of a phase III randomized trial comparing concurrent chemoradiotherapy with radiation therapy alone in patients with stage III and IV squamous cell carcinoma of the head and neck, Cancer 88(4) (2000) 876–83. [PubMed: 10679658]

[3]. Herskovic A, Martz K, al-Sarraf M, Leichman L, Brindle J, Vaitkevicius V, Cooper J, Byhardt R, Davis L, Emami B, Combined chemotherapy and radiotherapy compared with radiotherapy alone in patients with cancer of the esophagus, N Engl J Med 326(24) (1992) 1593–8. [PubMed: 1584260]

[4]. Epidermoid anal cancer: results from the UKCCCR randomised trial of radiotherapy alone versus radiotherapy, 5-fluorouracil, and mitomycin. UKCCCR Anal Cancer Trial Working Party. UK Coordinating Committee on Cancer Research, Lancet 348(9034) (1996) 1049–54. [PubMed: 8874455]

[5]. Al-Sarraf M, LeBlanc M, Giri PG, Fu KK, Cooper J, Vuong T, Forastiere AA, Adams G, Sakr WA, Schuller DE, Ensley JF, Chemoradiotherapy versus radiotherapy in patients with advanced nasopharyngeal cancer: phase III randomized Intergroup study 0099, J Clin Oncol 16(4) (1998) 1310–7. [PubMed: 9552031]

[6]. Morris M, Eifel PJ, Lu J, Grigsby PW, Levenback C, Stevens RE, Rotman M, Gershenson DM, Mutch DG, Pelvic radiation with concurrent chemotherapy compared with pelvic and para-aortic radiation for high-risk cervical cancer, N Engl J Med 340(15) (1999) 1137–43. [PubMed: 10202164]

[7]. Furuse K, Fukuoka M, Kawahara M, Nishikawa H, Takada Y, Kudoh S, Katagami N, Ariyoshi Y, Phase III study of concurrent versus sequential thoracic radiotherapy in combination with mitomycin, vindesine, and cisplatin in unresectable stage III non-small-cell lung cancer, J Clin Oncol 17(9) (1999) 2692–9. [PubMed: 10561343]

[8]. Macdonald JS, Smalley SR, Benedetti J, Hundahl SA, Estes NC, Stemmermann GN, Haller DG, Ajani JA, Gunderson LL, Jessup JM, Martenson JA, Chemoradiotherapy after surgery compared with surgery alone for adenocarcinoma of the stomach or gastroesophageal junction, N Engl J Med 345(10) (2001) 725–30. [PubMed: 11547741]

[9]. Moding EJ, Kastan MB, Kirsch DG, Strategies for optimizing the response of cancer and normal tissues to radiation, Nat Rev Drug Discov 12(7) (2013) 526–42. [PubMed: 23812271]

[10]. Liauw SL, Connell PP, Weichselbaum RR, New paradigms and future challenges in radiation oncology: an update of biological targets and technology, Sci Transl Med 5(173) (2013) 173sr2. [PubMed: 23427246]

[11]. Falls KC, Sharma RA, Lawrence YR, Amos RA, Advani SJ, Ahmed MM, Vikram B, Coleman CN, Prasanna PG, Radiation-Drug Combinations to Improve Clinical Outcomes and Reduce Normal Tissue Toxicities: Current Challenges and New Approaches: Report of the Symposium Held at the 63rd Annual Meeting of the Radiation Research Society, 15–18 October 2017; Cancun, Mexico, Radiat Res 190(4) (2018) 350–360. [PubMed: 30280985]

[12]. Khan MK, Nasti TH, Buchwald ZS, Weichselbaum RR, Kron SJ, Repurposing Drugs for Cancer Radiotherapy: Early Successes and Emerging Opportunities, Cancer J 25(2) (2019) 106–115. [PubMed: 30896532]

[13]. Lin SH, George TJ, Ben-Josef E, Bradley J, Choe KS, Edelman MJ, Guha C, Krishnan S, Lawrence TS, Le QT, Lu B, Mehta M, Peereboom D, Sarkaria J, Seong J, Wang D, Welliver MX, Coleman CN, Vikram B, Yoo S, Chung CH, Participants P on Workshop for, R. Clinical Development of, I. National Cancer, Opportunities and challenges in the era of molecularly targeted agents and radiation therapy, J Natl Cancer Inst 105(10) (2013) 686–93. [PubMed: 23503600]

[14]. Liu FF, p. worpkshop, Okunieff P, Bernhard EJ, Stone HB, Yoo S, Coleman CN, Vikram B, Brown M, Buatti J, Guha C, Lessons learned from radiation oncology clinical trials, Clin Cancer Res 19(22) (2013) 6089–100. [PubMed: 24043463]

[15]. Sharma RA, Plummer R, Stock JK, Greenhalgh TA, Ataman O, Kelly S, Clay R, Adams RA, Baird RD, Billingham L, Brown SR, Buckland S, Bulbeck H, Chalmers AJ, Clack G, Cranston AN, Damstrup L, Ferraldeschi R, Forster MD, Golec J, Hagan RM, Hall E, Hanauske AR, Harrington KJ, Haswell T, Hawkins MA, Illidge T, Jones H, Kennedy AS, McDonald F, Melcher T, O'Connor JP, Pollard JR, Saunders MP, Sebag-Montefiore D, Smitt M, Staffurth J, Stratford IJ, Wedge SR, N.C.A.-P.J.W. Group, Clinical development of new drug-radiotherapy combinations, Nat Rev Clin Oncol 13(10) (2016) 627–42. [PubMed: 27245279]

[16]. Bristow RG, Alexander B, Baumann M, Bratman SV, Brown JM, Camphausen K, Choyke P, Citrin D, Contessa JN, Dicker A, Kirsch DG, Krause M, Le QT, Milosevic M, Morris ZS, Sarkaria JN, Sondel PM, Tran PT, Wilson GD, Willers H, Wong RKS, Harari PM, Combining precision radiotherapy with molecular targeting and immunomodulatory agents: a guideline by the American Society for Radiation Oncology, Lancet Oncol 19(5) (2018) e240–e251. [PubMed: 29726389]

[17]. Kesari S, Advani SJ, Lawson JD, Kahle KT, Ng K, Carter B, Chen CC, DNA damage response and repair: insights into strategies for radiation sensitization of gliomas, Future Oncol 7(11) (2011) 1335–46. [PubMed: 22044206]

[18]. Buckel L, Savariar EN, Crisp JL, Jones KA, Hicks AM, Scanderbeg DJ, Nguyen QT, Sicklick JK, Lowy AM, Tsien RY, Advani SJ, Tumor radiosensitization by monomethyl auristatin E: mechanism of action and targeted delivery, Cancer Res 75(7) (2015) 1376–1387. [PubMed: 25681274]

[19]. Adams SR, Yang HC, Savariar EN, Aguilera J, Crisp JL, Jones KA, Whitney MA, Lippman SM, Cohen EE, Tsien RY, Advani SJ, Anti-tubulin drugs conjugated to anti-ErbB antibodies selectively radiosensitize, Nat Commun 7 (2016) 13019. [PubMed: 27698471]

[20]. Hingorani DV, Doan MK, Camargo MF, Aguilera J, Song SM, Pizzo D, Scanderbeg DJ, Cohen EEW, Lowy AM, Adams SR, Advani SJ, Precision Chemo-Radiotherapy for HER2 Tumors Using Antibody Conjugates of an Auristatin Derivative with Reduced Cell Permeability, Mol Cancer Ther (2019).

[21]. Lambert JM, Berkenblit A, Antibody-Drug Conjugates for Cancer Treatment, Annu Rev Med 69 (2018) 191–207. [PubMed: 29414262]

[22]. Younes A, Bartlett NL, Leonard JP, Kennedy DA, Lynch CM, Sievers EL, Forero-Torres A, Brentuximab vedotin (SGN-35) for relapsed CD30-positive lymphomas, N Engl J Med 363(19) (2010) 1812–21. [PubMed: 21047225]

[23]. Verma S, Miles D, Gianni L, Krop IE, Welslau M, Baselga J, Pegram M, Oh DY, Dieras V, Guardino E, Fang L, Lu MW, Olsen S, Blackwell K, Group ES, Trastuzumab emtansine for HER2positive advanced breast cancer, N Engl J Med 367(19) (2012) 1783–91. [PubMed: 23020162]

[24]. Palanca-Wessels MC, Czuczman M, Salles G, Assouline S, Sehn LH, Flinn I, Patel MR, Sangha R, Hagenbeek A, Advani R, Tilly H, Casasnovas O, Press OW, Yalamanchili S, Kahn R, Dere RC, Lu D, Jones S, Jones C, Chu YW, Morschhauser F, Safety and activity of the antiCD79B antibody-drug conjugate polatuzumab vedotin in relapsed or refractory B-cell non-Hodgkin lymphoma and chronic lymphocytic leukaemia: a phase 1 study, Lancet Oncol 16(6) (2015) 704–15. [PubMed: 25925619]

[25]. Amadori S, Suciu S, Selleslag D, Aversa F, Gaidano G, Musso M, Annino L, Venditti A, Voso MT, Mazzone C, Magro D, De Fabritiis P, Muus P, Alimena G, Mancini M, Hagemeijer A, Paoloni F, Vignetti M, Fazi P, Meert L, Ramadan SM, Willemze R, de Witte T, Baron F, Gemtuzumab Ozogamicin Versus Best Supportive Care in Older Patients With Newly Diagnosed

Acute Myeloid Leukemia Unsuitable for Intensive Chemotherapy: Results of the Randomized Phase III EORTC-GIMEMA AML-19 Trial, J Clin Oncol 34(9) (2016) 972–9. [PubMed: 26811524]

[26]. Kantarjian HM, DeAngelo DJ, Stelljes M, Liedtke M, Stock W, Gokbuget N, O'Brien SM, Jabbour E, Wang T, Liang White J, Sleight B, Vandendries E, Advani AS, Inotuzumab ozogamicin versus standard of care in relapsed or refractory acute lymphoblastic leukemia: Final report and longterm survival follow-up from the randomized, phase 3 INO-VATE study, Cancer 125(14) (2019) 2474–2487. [PubMed: 30920645]

[27]. Tripathi PP, Arami H, Banga I, Gupta J, Gandhi S, Cell penetrating peptides in preclinical and clinical cancer diagnosis and therapy, Oncotarget 9(98) (2018) 37252–37267. [PubMed: 30647857]

[28]. Jiang T, Olson ES, Nguyen QT, Roy M, Jennings PA, Tsien RY, Tumor imaging by means of proteolytic activation of cell-penetrating peptides, Proc Natl Acad Sci U S A 101(51) (2004) 17867–72. [PubMed: 15601762]

[29]. Mitchell JB, Choudhuri R, Fabre K, Sowers AL, Citrin D, Zabludoff SD, Cook JA, In vitro and in vivo radiation sensitization of human tumor cells by a novel checkpoint kinase inhibitor, AZD7762, Clin Cancer Res 16(7) (2010) 2076–84. [PubMed: 20233881]

[30]. Morgan MA, Parsels LA, Zhao L, Parsels JD, Davis MA, Hassan MC, Arumugarajah S, Hylander-Gans L, Morosini D, Simeone DM, Canman CE, Normolle DP, Zabludoff SD, Maybaum J, Lawrence TS, Mechanism of radiosensitization by the Chk1/2 inhibitor AZD7762 involves abrogation of the G2 checkpoint and inhibition of homologous recombinational DNA repair, Cancer Res 70(12) (2010) 4972–81. [PubMed: 20501833]

[31]. Advani SJ, Camargo MF, Seguin L, Mielgo A, Anand S, Hicks AM, Aguilera J, Franovic A, Weis SM, Cheresh DA, Kinase-independent role for CRAF-driving tumour radioresistance via CHK2, Nat Commun 6 (2015) 8154. [PubMed: 26333361]

[32]. Doronina SO, Bovee TD, Meyer DW, Miyamoto JB, Anderson ME, Morris-Tilden CA, Senter PD, Novel peptide linkers for highly potent antibody-auristatin conjugate, Bioconjug Chem 19(10) (2008) 1960–3. [PubMed: 18803412]

[33]. Aguilera TA, Olson ES, Timmers MM, Jiang T, Tsien RY, Systemic in vivo distribution of activatable cell penetrating peptides is superior to that of cell penetrating peptides, Integr Biol (Camb) 1(5–6) (2009) 371–81. [PubMed: 20023744]

[34]. Olson ES, Aguilera TA, Jiang T, Ellies LG, Nguyen QT, Wong EH, Gross LA, Tsien RY, In vivo characterization of activatable cell penetrating peptides for targeting protease activity in cancer, Integr Biol (Camb) 1(5–6) (2009) 382–93. [PubMed: 20023745]

[35]. Crisp JL, Savariar EN, Glasgow HL, Ellies LG, Whitney MA, Tsien RY, Dual targeting of integrin alphavbeta3 and matrix metalloproteinase-2 for optical imaging of tumors and chemotherapeutic delivery, Mol Cancer Ther 13(6) (2014) 1514–25. [PubMed: 24737028]

[36]. Roy R, Yang J, Moses MA, Matrix metalloproteinases as novel biomarkers and potential therapeutic targets in human cancer, J Clin Oncol 27(31) (2009) 5287–97. [PubMed: 19738110]

[37]. Savariar EN, Felsen CN, Nashi N, Jiang T, Ellies LG, Steinbach P, Tsien RY, Nguyen QT, Real-time in vivo molecular detection of primary tumors and metastases with ratiometric activatable cell-penetrating peptides, Cancer Res 73(2) (2013) 855–64. [PubMed: 23188503]

[38]. Deryugina EI, Ratnikov B, Monosov E, Postnova TI, DiScipio R, Smith JW, Strongin AY, MT1-MMP initiates activation of pro-MMP-2 and integrin alphavbeta3 promotes maturation of MMP-2 in breast carcinoma cells, Exp Cell Res 263(2) (2001) 209–23. [PubMed: 11161720]

[39]. Winer A, Adams S, Mignatti P, Matrix Metalloproteinase Inhibitors in Cancer Therapy: Turning Past Failures Into Future Successes, Mol Cancer Ther 17(6) (2018) 1147–1155. [PubMed: 29735645]

[40]. Raju SC, Hauff SJ, Lemieux AJ, Orosco RK, Gross AM, Nguyen LT, Savariar E, Moss W, Whitney M, Cohen EE, Lippman SM, Tsien RY, Ideker T, Advani SJ, Nguyen QT, Combined TP53 mutation/3p loss correlates with decreased radiosensitivity and increased matrixmetalloproteinase activity in head and neck carcinoma, Oral Oncol 51(5) (2015) 470–5. [PubMed: 25735654]

[41]. Kumar A, Collins HM, Scholefield JH, Watson SA, Increased type-IV collagenase (MMP-2 and MMP-9) activity following preoperative radiotherapy in rectal cancer, Br J Cancer 82(4) (2000) 960–5. [PubMed: 10732772]

[42]. Zhao W, Goswami PC, Robbins ME, Radiation-induced up-regulation of Mmp2 involves increased mRNA stability, redox modulation, and MAPK activation, Radiat Res 161(4) (2004) 418–29. [PubMed: 15038770]

[43]. Chou CH, Teng CM, Tzen KY, Chang YC, Chen JH, Cheng JC, MMP-9 from sublethally irradiated tumor promotes Lewis lung carcinoma cell invasiveness and pulmonary metastasis, Oncogene 31(4) (2012) 458–68. [PubMed: 21706046]

[44]. Chetty C, Bhoopathi P, Rao JS, Lakka SS, Inhibition of matrix metalloproteinase-2 enhances radiosensitivity by abrogating radiation-induced FoxM1-mediated G2/M arrest in A549 lung cancer cells, Int J Cancer 124(10) (2009) 2468–77. [PubMed: 19165865]

[45]. Appelbe OK, Zhang Q, Pelizzari CA, Weichselbaum RR, Kron SJ, Image-Guided Radiotherapy Targets Macromolecules through Altering the Tumor Microenvironment, Mol Pharm 13(10) (2016) 3457–3467. [PubMed: 27560921]

[46]. Kapoor V, Singh AK, Rogers BE, Thotala D, Hallahan DE, PEGylated peptide to TIP1 is a novel targeting agent that binds specifically to various cancers in vivo, J Control Release 298 (2019) 194–201. [PubMed: 30763622]

[47]. Yan H, Kapoor V, Nguyen K, Akers WJ, Li H, Scott J, Laforest R, Rogers B, Thotala D, Hallahan D, Anti-tax interacting protein-1 (TIP-1) monoclonal antibody targets human cancers, Oncotarget 7(28) (2016) 43352–43362. [PubMed: 27270318]

[48]. Birmingham A, Selfors LM, Forster T, Wrobel D, Kennedy CJ, Shanks E, Santoyo-Lopez J, Dunican DJ, Long A, Kelleher D, Smith Q, Beijersbergen RL, Ghazal P, Shamu CE, Statistical methods for analysis of high-throughput RNA interference screens, Nat Methods 6(8) (2009) 569–75. [PubMed: 19644458]

Highlights

- Cell penetrating peptide (CPP) drug conjugates radiosensitize.
- Activatable cell penetrating peptide (ACPP) engineered scaffolding cloaks CPPs.
- Tumor overexpressed extracellular proteases cleave ACPPs and guide CPP delivery.
- ACPP scaffolds increase tumor targeting and decreases normal tissue accumulation.
- Radiosensitizers conjugated to ACPP given with radiotherapy increase tumor control.

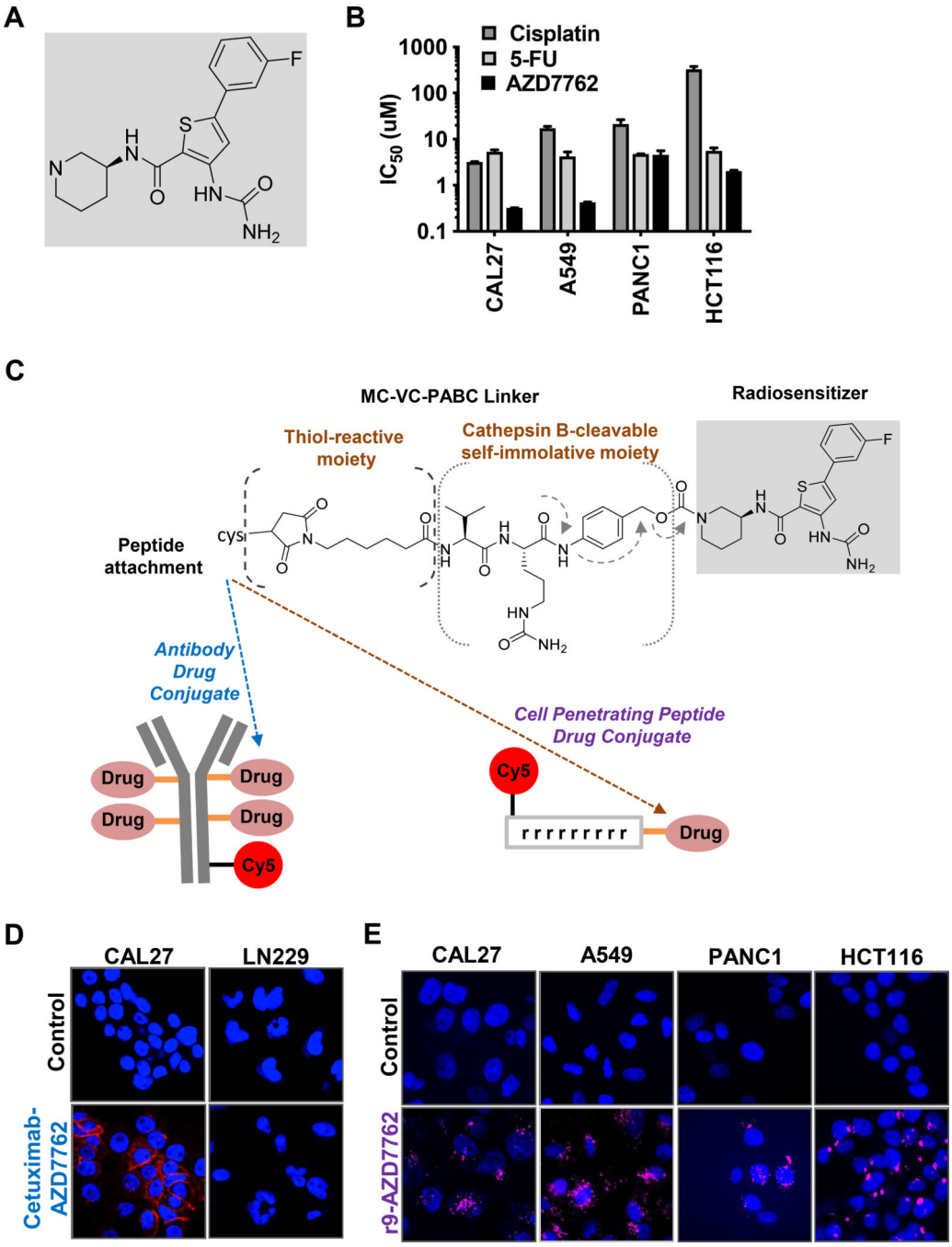

Figure 1: Peptide linker conjugation of AZD7762.

(A) Structure of DNA damage checkpoint kinase inhibitor AZD7762. (B) IC_{50} of AZD7762 compared to cisplatin and 5-fluorouracil (5-FU). CAL27, A549, PANC1 and HCT116 cells exposed to a dose range of drug. Cell survival measured by Alamar Blue assay and IC_{50} calculated. Data plotted as mean IC_{50} ± SD. (C) Schema for synthesizing antibody and cell penetrating peptide conjugates of AZD7762 through a maleimidocaproyl-valine-citrulline-paminobenzyl carbamyl linker (MC-VC-PABC). Antibody drug conjugate synthesized with four MC-VCPABC linked drug molecules per antibody. Polycationic cell penetrating peptide

drug conjugate synthesized by attaching one MC-VC-PABC linked drug molecule to a nine D-arginine polypeptide repeat. Drug carriers were Cy5 labeled. (D) Cetuximab-AZD7762 conjugate binding to cancer cells. EGFR expressing (CAL27) and EGFR negative (LN229) tumor cells exposed to 2 nM CetuximabAZD7762, fixed and imaged for Cy5 fluorescence (red). Nuclei DAPI stained (blue). White scale bar, 10 μM. (E) AZD7762 cell penetrating peptide drug conjugates uptake across tumor histologies. Tumor cells exposed to 100 nM r9-AZD7762. Cells fixed and imaged for Cy5 fluorescence (red). Nuclei DAPI stained (blue). White scale bar, 10 μM.

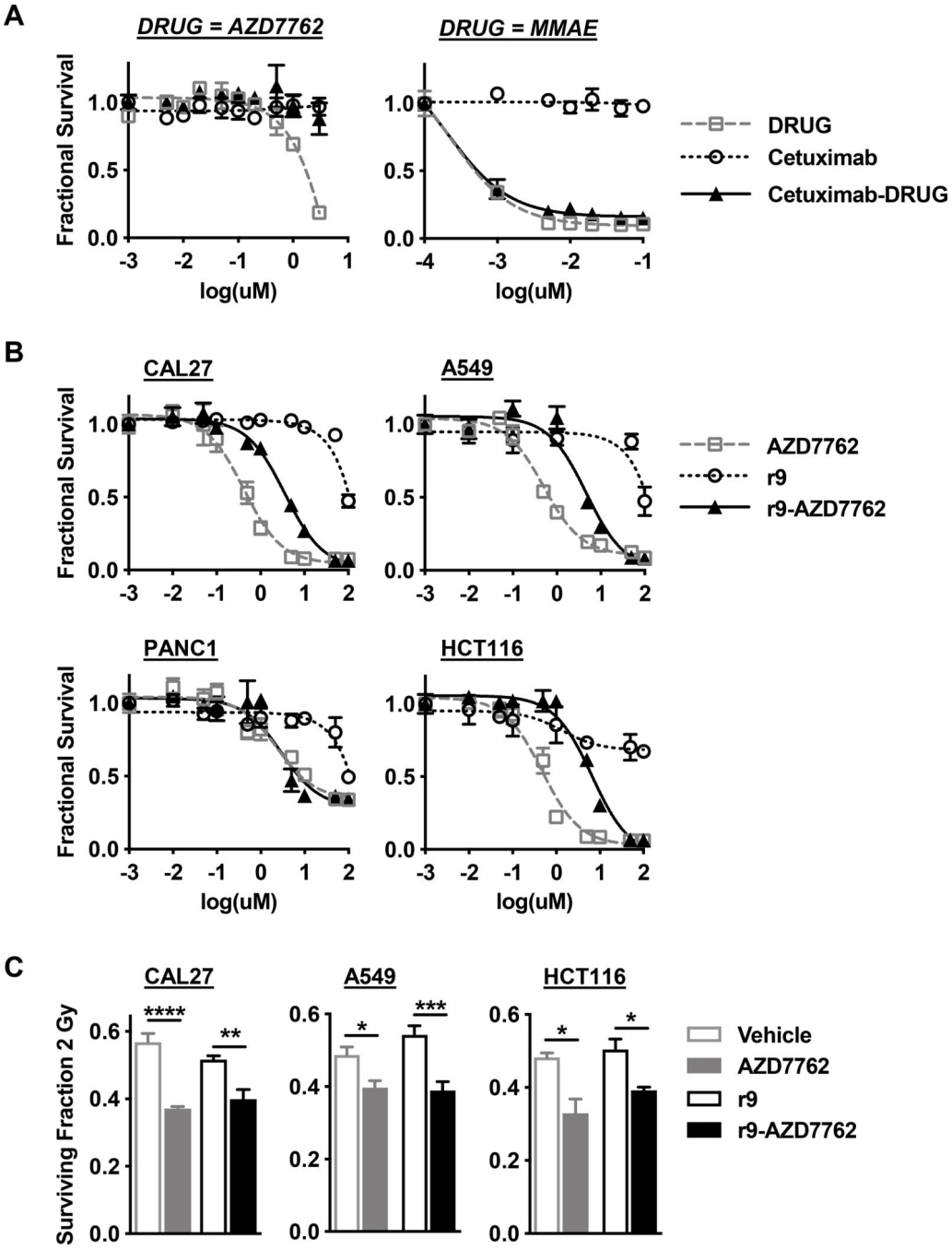

Figure 2: Cytotoxicity and radiosensitization of AZD7762 conjugates.

(A) CAL27 cells exposed to a dose range of cetuximab, free drug (AZD7762 or monomethyl auristatin E (MMAE)) or antibody drug conjugates for 72 hrs. Cell viability measured by Alamar Blue assay, normalized to control untreated cells and plotted as mean fractional survival ± SD. (B) Tumor cells exposed to a dose range of free AZD7762, r9 peptide alone or r9-drug conjugate for 72 hrs. Cell viability measured by Alamar Blue assay, normalized to control untreated cells and plotted as mean fractional survival ± SD. (C) Clonogenic cell survival of tumor cells treated with 50 nM of drug, free peptide or r9 drug conjugate for 1 hr.

and then irradiated with 2 Gy. Cell viability normalized to non-irradiated cells for each drug condition and plotted as mean fractional survival after 2 Gy ± SEM. *P<0.05, **P<0.01, ***P<0.001, ****P<0.0001.

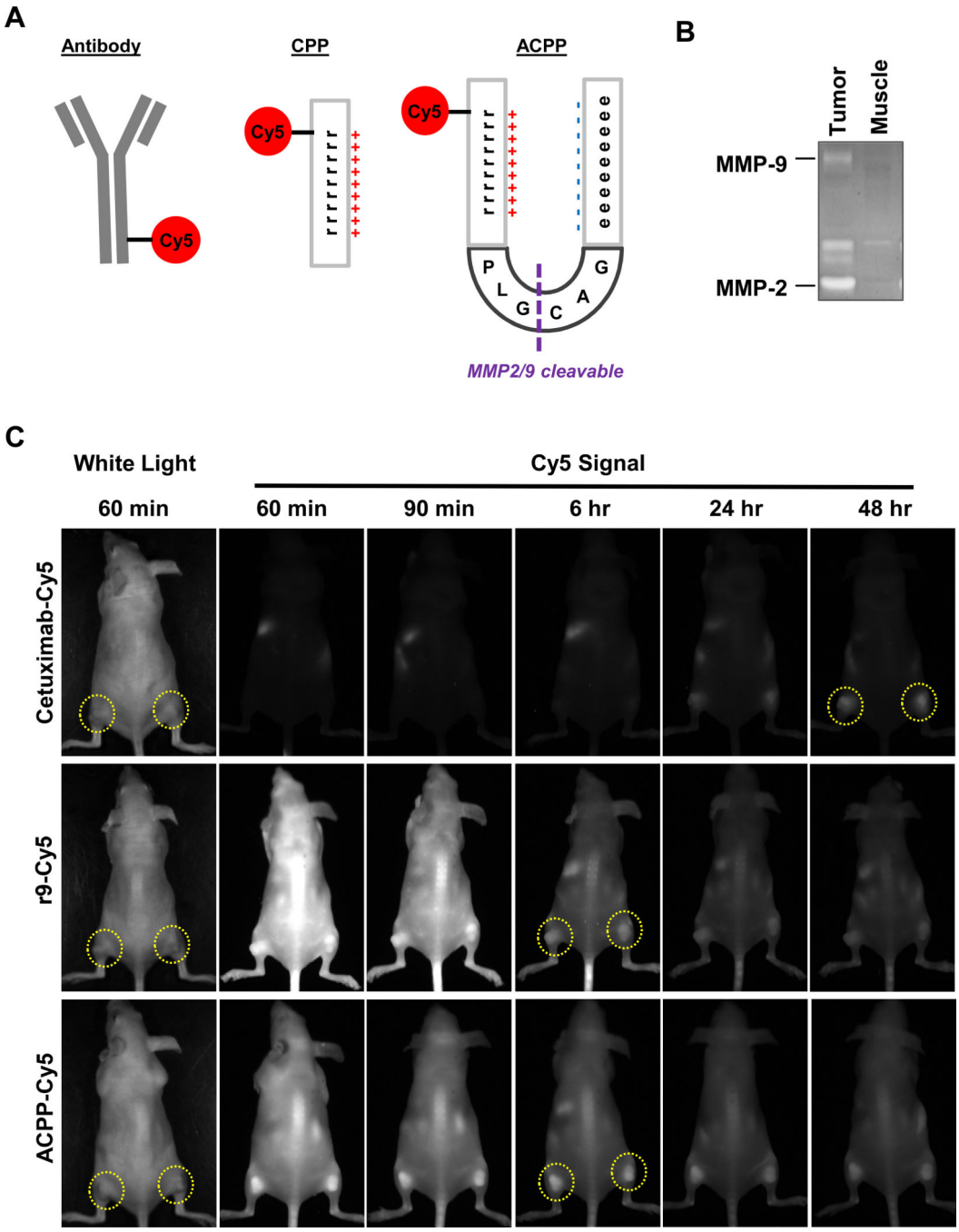

Figure 3: Fluorescent labeled antibody and cell penetrating peptide distribution *in vivo*.

(A) Structural representation of Cy5 labeled cetuximab antibody, polycationic r9 cell penetrating peptide (CPP) or activatable cell penetrating peptide (ACPP). ACPP has polycationic cell penetrating and polyanionic peptides separated by a MMP-2/9 cleavable PLGC(Me)AG peptide linker. (B) MMP-2/9 gelatinase activity of tissue from athymic nude mice with subcutaneous CAL27 human tumor xenografts. Gelatin zymography of excised tumor tissue and adjacent muscle tissue. MMP-2 and MMP-9 standard activities indicated by left side markers. (C) Mice with subcutaneous CAL27 tumors tail vein injected with Cy5

labeled cetuximab, r9 or ACPP. Mice serially imaged for Cy5 fluorescence (white signal) post injection. White light images of mice show tumor locations in bilateral thighs (yellow circles).

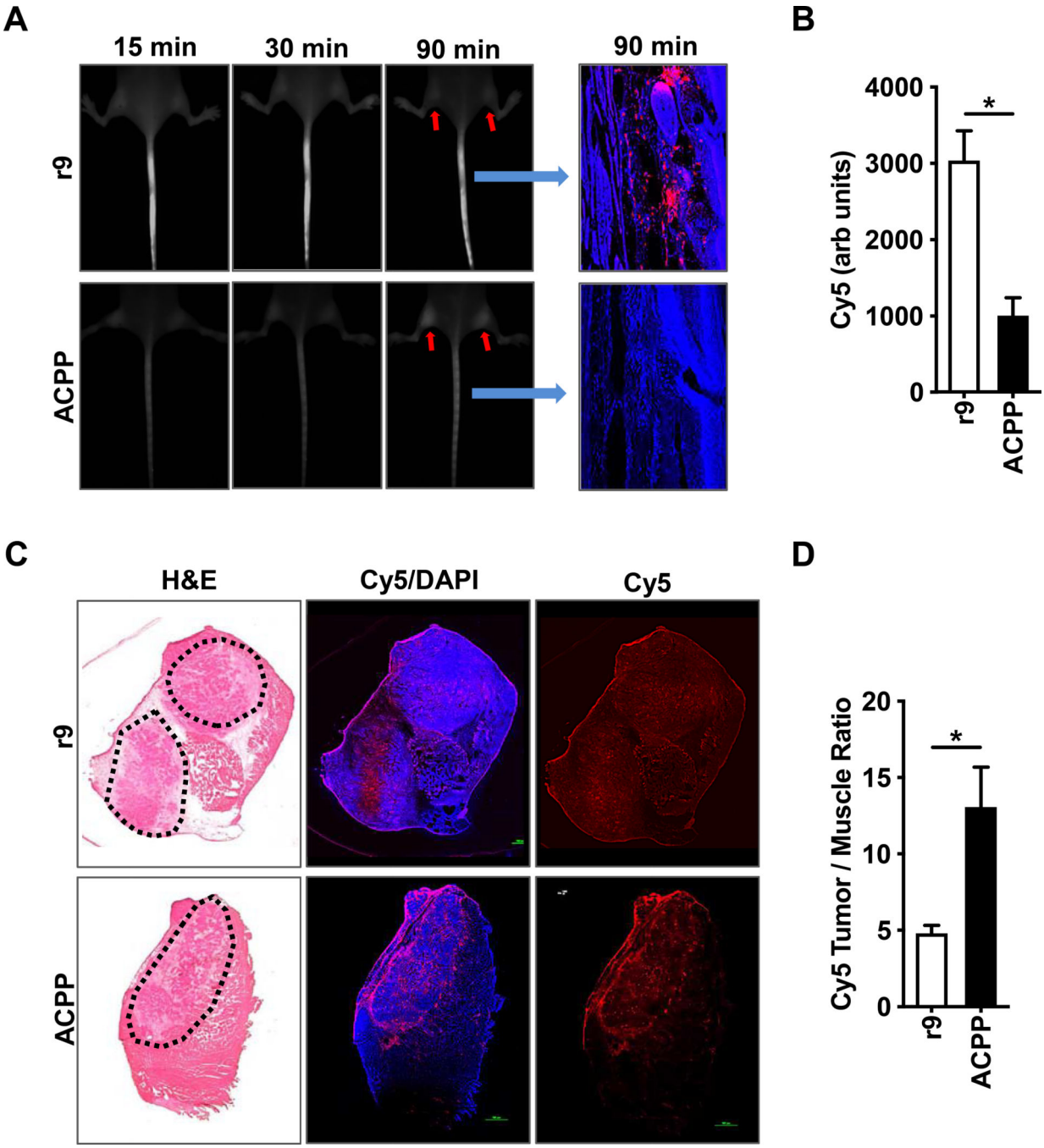

Figure 4: ACPP cloaked cell penetrating peptide tissue localization.

Mice with subcutaneous CAL27 tumors tail vein injected with 10 nanomoles Cy5 labeled r9 or ACPP. (A) Mice serially imaged for Cy5 fluorescence (white signal) post injection. At 90 minutes, tails harvested, sectioned, DAPI stained (blue) and imaged for Cy5 (red), blue arrows. Red arrows show location of bilateral thigh tumors. (B) Cy5 signal quantitated in tail sections and plotted as mean ± SEM. (C) Tissue containing both subcutaneous tumor and underlying normal muscle harvested 90 minutes after Cy5 labeled r9 or ACPP peptide tail vein injected. Tumor tissue (enclosed within circles) and normal muscle delineated by H&E

staining. Tissue sections DAPI stained (blue), direct Cy5 peptide signal captured (red). (D) Cy5 signal quantitated in tumor and adjacent muscle. Data plotted as mean Cy5 signal ratio in tumor to muscle ± SEM. *P<0.05.

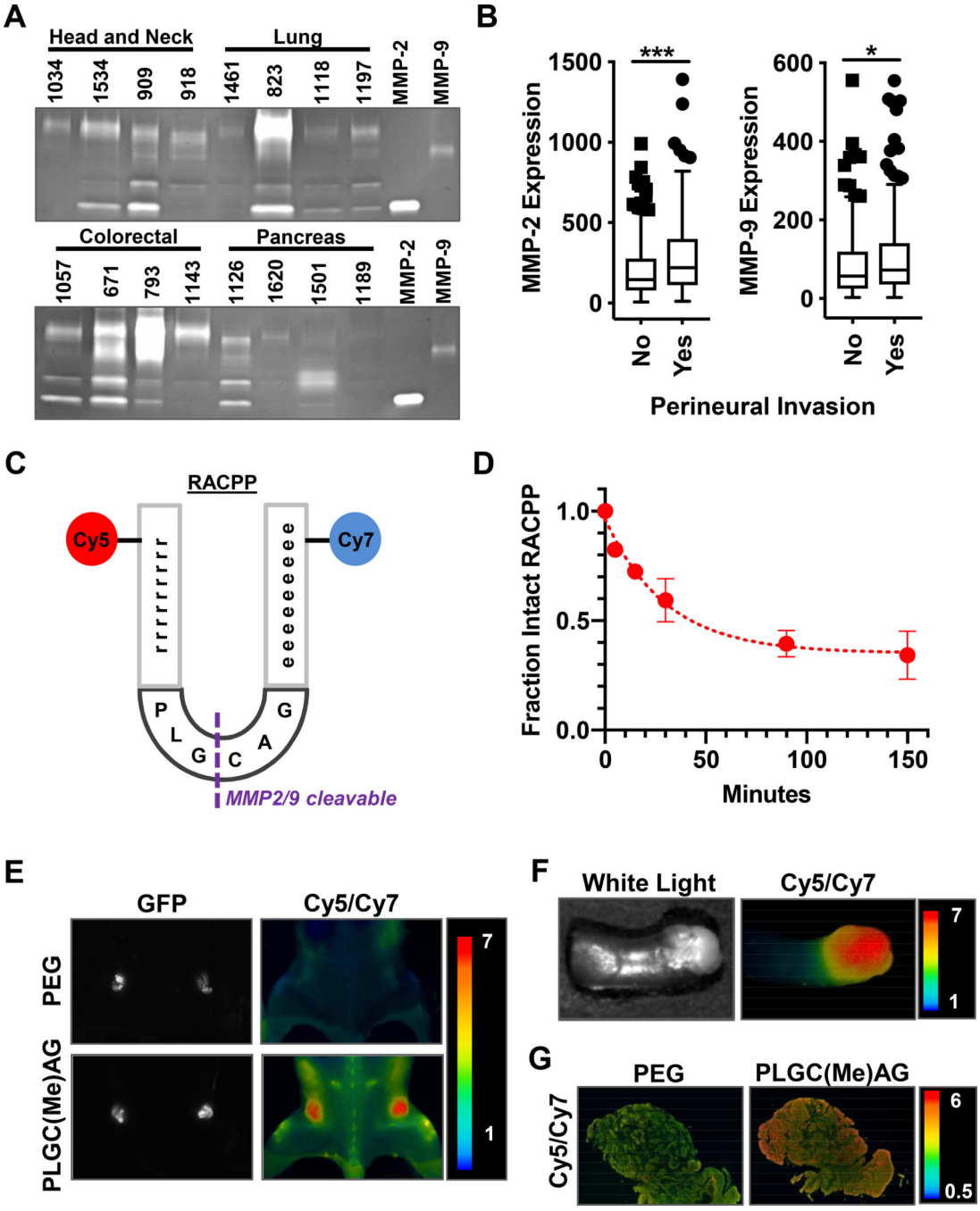

Figure 5: Tumor specific cleavage of ACPP *in situ*.

(A) Gelatin zymography assay of patient tumor samples from histologies routinely treated with concurrent chemotherapy and radiotherapy. For each histology, 4 unique de-identified patient samples were tested. MMP-2 and MMP-9 standard activities in far right lanes. (B) Correlation of MMP-2 and MMP-9 expression with perineural tumor invasion in patient tumor tissue. Level 3 normalized mRNA expression read counts for tumor samples from 500 head and neck squamous cell cancer patients analyzed from The Cancer Genome Atlas (TCGA). (C) Structural representation of ratiometric activatable cell penetrating peptide

(RACPP) probe with intervening MMP-2/9 protease sensitive amino acid sequence. Cy5 attached to the polycationic cell penetrating peptide and Cy7 to the polyanionic peptide ends of ACPP. (D) MMP cleavage of RACPP. RACPP incubated with human recombinant MMP-9. At time points an aliquot was analyzed by LC-MS for Cy5 signal on intact RACPP remaining. Data normalized to RACPP Cy5 signal prior to MMP-9 addition (time 0) and plotted as mean ± SD. (E) Mice with subcutaneous GFP expressing CAL27 tumors tail vein injected with 10 nanomoles ratiometric ACPP containing a non-cleavable polyethylene glycol linker (PEG) or MMP-2/9 cleavable linker (PLGC(Me)AG). *In situ* mouse imaging for GFP, Cy5 and Cy7 direct fluorescence with Cy5:Cy7 emission ratio determined (pseudocolor scale bar far right). (F) Orthotopic CAL27 tumor established in a mouse tongue and 10 nanomoles ratiometric ACPP i.v. injected. Whole tongue excised 90 minutes later and imaged under white light and for Cy5 and Cy7 fluorescence with Cy5:Cy7 emission ratio determined (pseudocolor scale bar far right). (G) Tumor biopsy specimens from a patient with poorly differentiated squamous cell head and neck cancer incubated with 10 μM ratiometric ACPP containing a PEG or PLGC(Me)AG linker. Cy5 and Cy7 fluorescence captured and Cy5:Cy7 emission ratio determined (pseudocolor scale bar far right). *P<0.05, ***P<0.001.

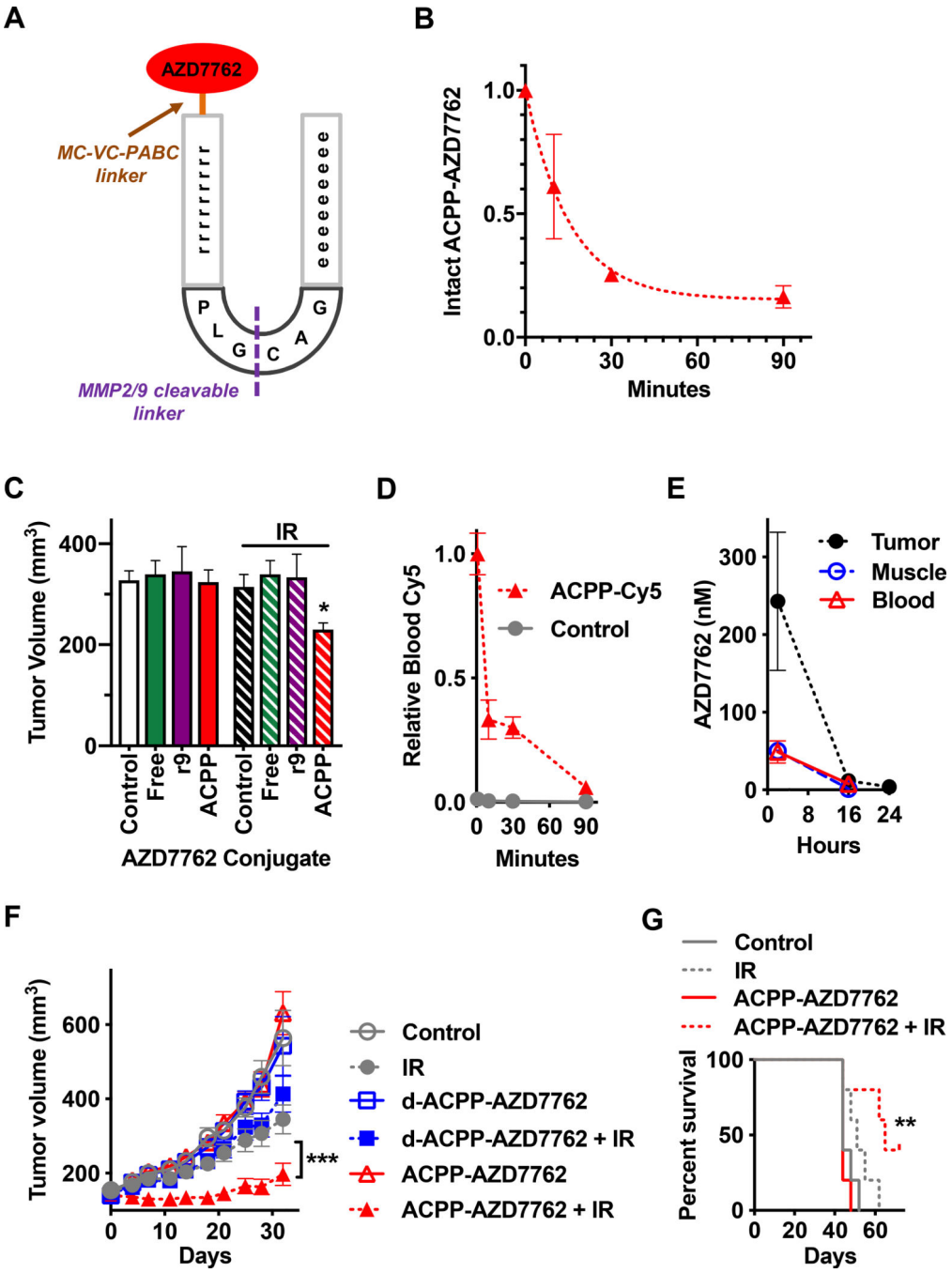

Figure 6: Radiotherapy and ACPP conjugated AZD7762 improves tumor control.

(A) Structural representation of AZD7762 conjugated to ACPP. (B) MMP cleavage of ACPP-AZD7762. ACPP-AZD7762 was incubated with human recombinant MMP-9. At time points an aliquot was analyzed by LC-MS for intact ACPP-AZD7762 remaining. Data normalized to ACPP-AZD7762 signal prior to MMP-9 addition (time 0) and plotted as mean ± SD. (C) Mice bearing CAL27 tumors i.v. injected with vehicle (control) or 60 nanomoles AZD7762 on day 0. AZD7762 tested as a free drug or peptide conjugate to r9 cell penetrating peptide and ACPP. Four Gy of IR was focally delivered to tumor bearing

hindlimbs on days 0 and 1. Tumors volumes on day 14 plotted as mean tumor volume ± SEM. Statistical significances calculated using one-way ANOVA. (D) Kinetics of ACPP blood clearance. Mice with CAL27 tumors i.v. injected with water (control) or 10 nanomoles Cy5 labeled ACPP. Blood collected at indicated time points, Cy5 signal measured and data plotted as mean ± SEM. (E) Temporal biodistribution of AZD7762 ACPP conjugate in tumor bearing mice. Mice with CAL27 tumors i.v. injected with 100 nanomoles of ACPP-AZD7762. Tissues and blood harvested at indicated times and AZD7762 drug concentration quantitated by LC-MS/MS. Data plotted as mean ± SEM. (F) Necessity of ACPP cleavage for anti-tumor efficacy of conjugated radiosensitizer. Mice with PANC1 tumor xenografts injected with 100 nmoles of cleavable or non-cleavable ACPP conjugates of AZD7762 on day 0 and 3. d-ACPP-AZD7762 synthesized with L-amino acid ACPP peptide linker replaced by biologically inert D-amino acids and cRGD replaced by cRAD. For IR, 3 Gy given to tumors on days 0,1, 3, 4 and 5. Tumors measured twice a week and plotted as mean tumor volume ± SEM. Statistical significances calculated using two-way ANOVA with Tukey's multiple comparisons test. (G) Mice with CAL27 tumors i.v. injected with 200 nanomoles of ACPP conjugated to AZD7762 on day 0, 1 and 2. For IR, 3 Gy focally given to tumors on days 0, 1 and 2. Mouse survival plotted and statistical significances calculated using Log-rank (Mantel-Cox) test. **P<0.01, ***P<0.001.